Available online at www.sciencedirect.com
ScienceDirect
Journal of Sound and Vibration 322 (2009) 196–215
JOURNAL OF SOUND AND VIBRATION
www.elsevier.com/locate/jsvi

Vibration displacement on substrate due to time-harmonic stress sources from a micromechanical resonator

Zhili Hao*, Yang Xu

Department of Mechanical Engineering, Old Dominion University, 238 Kaufman Hall, Norfolk, VA 23529-0247, USA

Received 14 December 2007; received in revised form 17 October 2008; accepted 7 November 2008
Handling Editor: S. Bolton
Available online 21 December 2008

Abstract

This paper investigates the vibration displacement on substrate due to time-harmonic stress sources from a micromechanical resonator fabricated using Microelectromechanical Systems (MEMS) technology. The vibrations of a micromechanical resonator exert a time-harmonic stress across the clamped region on its substrate and further excite elastic waves propagating into the substrate, therefore leading to the dissipation of vibration energy—commonly referred to as support loss. Support loss can be quantitatively evaluated in terms of this time-harmonic stress and its corresponding vibration displacement on substrate. To calculate this vibration displacement, this work treats the substrate as either a semi-infinite or infinite elastic medium. Then, the classic elastic wave theories are utilized to describe its behavior, and the Fourier transform or Hankel transform is employed for dealing with the geometrical infinity of the substrate. Consequently, the mathematical expressions for this vibration displacement, under several typical time-harmonic stress sources in micromechanical resonators, are derived. As a result, this work provides the basis for quantitatively evaluating support loss in a micromechanical resonator and predicts the relation of support loss versus some key resonator design parameters and substrate materials.

1. Introduction

Due to their small size, low-cost batch fabrication and low power consumption, micromechanical resonators fabricated using Microelectromechanical Systems (MEMS) technology have been of great interests for a wide range of sensing and wireless communication applications [1–11], where micromechanical resonators function as accelerometers [1], gyroscopes [2,3], oscillators [4,5], or electrical filters [6–11]. For their practical applications, energy loss mechanisms or quality factors (Q) of micromechanical resonators are of critical importance, as a higher Q in such devices translates to higher sensitivity, better bias stability, and improved resolution [2–4]. Therefore, these micromechanical resonators are preferred (also feasible due to their small size) to be packaged in vacuum for operation so that air damping is eliminated. Consequently, support loss, thermoelastic damping (TED) and surface loss come to the fore and the overall measured Quality

*Corresponding author. Tel.: +1 757 683 6734; fax: +1 757 683 5344.
E-mail address: zlhao@odu.edu (Z. Hao).

0022-460X/$ - see front matter © 2008 Elsevier Ltd. All rights reserved.
doi:10.1016/j.jsv.2008.11.004

factor of a micromechanical resonator operating in vacuum is expressed as [12–14]:

$$\frac{1}{Q_{measured}} \cong \frac{1}{Q_{support}} + \frac{1}{Q_{TED}} + \frac{1}{Q_{surface}}. \quad (1)$$

Apparently, these three loss mechanisms become the major bottlenecks for these resonators' performance. Toward this end, one needs to understand energy loss mechanisms in such devices, not only for predicting the Q of a micromechanical resonator at the design stage, but also for improving their performance through design and fabrication tradeoff.

This work is aimed to aid in quantitatively addressing support loss in a micromechanical resonator and establishing the relation between support loss and the key design parameters of a resonator. The physical mechanism of support loss is illustrated in Fig. 1 [12,15]. Support loss, also known as anchor loss, is the portion of the vibration energy of a resonator dissipated by transmission through its support or substrate. During its vibrations, a micromechanical resonator exerts a time-harmonic stress across the clamped region on its substrate. Acting as an excitation source, this time-harmonic stress will further excite elastic waves propagating into the substrate. Part of the vibration energy dissipated through elastic wave propagation in support media—substrate is commonly referred to as *support loss*.

As will be described in the following section, support loss can be calculated in terms of the time-harmonic stress from a resonator and its corresponding vibration displacement on substrate. The time-harmonic stress from the vibrations of a micromechanical resonator can be easily obtained using a finite element modeling (FEM) tool, such as ANSYS. In contrast, the calculation of the vibration displacement on substrate imposes significant technical challenges, simply because of the extremely large geometry of the substrate relative to the clamped region of a resonator. Therefore, this paper focuses on providing a comprehensive derivation of the vibration displacement on substrate, under those typical time-harmonic stress sources in micromechanical resonators.

Fig. 2 shows a SEM (scanning electron microscope) picture of a portion of a die with micromechanical resonators sitting on top of the substrate. The in-plane dimension and thickness of the substrate (or the die) are typically $1\,\text{cm} \times 1\,\text{cm}$ and $500\,\mu\text{m}$, respectively. In contrast, the clamped region of a micromechanical resonator is typically $150\,\mu\text{m} \times 150\,\mu\text{m}$. As compared to the clamped region, the substrate is extremely large and thus can be treated as either a semi-infinite or an infinite medium. Then, we can utilize the large body of literature on the investigation of the vibration displacement on a semi-infinite or infinite elastic medium [16–20], which were originally developed for other applications (e.g., earthquake and acoustic emission) over the past century, to find out the vibration displacement on substrate that is particularly tailored to micromechanical resonators. Compared with the related work in the existing literature [16–20], our original contributions are: (1) this work presents the derivation of the vibration displacement on substrate in a much more accessible way than the corresponding original artworks published more than half century ago, for the purpose of making the derived formulas clear and beneficial to the MEMS community, where the elastic wave theories is not a very familiar topic. Accordingly, readers can choose the formulas suitable for their cases to predict support loss and improve the design of micromechanical resonators. (2) For the first time, the derivation of the vibration displacement on substrate is organized and the physical implication of the derived formulas is explored in the application context of micromechanical resonators. (3) The numerical values for the integrals involved in different configurations of micromechanical resonators are provided.

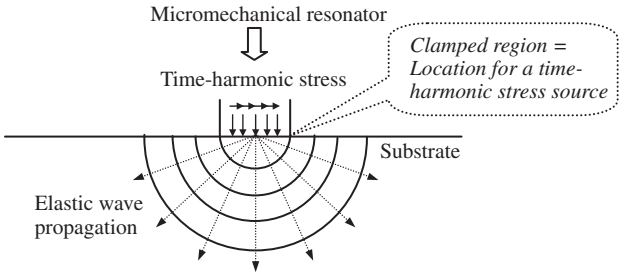

Fig. 1. Physical mechanism of support loss in a micromechanical resonator.

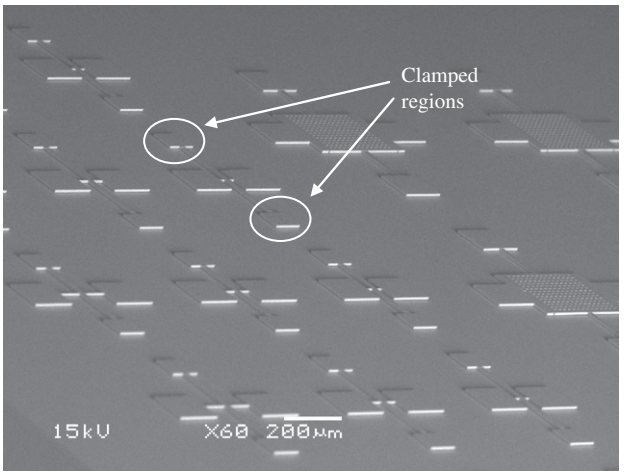

Fig. 2. A SEM picture of partial die of micromechanical resonators sitting on top of a silicon substrate.

This paper is organized as follows. Section 2 describes the fundamental assumptions for modeling support loss and two typical configurations of a micromechanical resonator with respect to its substrate, leading to different time-harmonic stress sources on a substrate. Then, Sections 3–5 review the classic elastic wave theories and combine different time-harmonic stress sources with the Fourier transform or Hankel transform to obtain the mathematical expressions for the vibration displacement on substrate. At the end, the results obtained from these three sections are summarized and discussed, providing the mathematical expressions for calculating support loss in a micromechanical resonator as well as the relation of support loss versus some key resonator design parameters and substrate materials.

2. Fundamental assumptions and two typical configurations of a micromechanical resonator with respect to its substrate

2.1. Fundamental assumptions

As described above, the vibrations of a micromechanical resonator cause a time-harmonic stress at the clamped region and then this stress excites the elastic waves propagating in the substrate. It has been theoretically proved [21] that, when the wavelength of the propagating elastic wave is much larger than the size of a clamped region, the coupling between the vibration modes of a micromechanical resonator and the elastic wave modes in its substrate is very weak and hence the energy transmission from the clamped region to the substrate can be treated as perturbation. Therefore, a resonator and its substrate can be separated and the time-harmonic stress at the clamped region from the resonator can be treated as the excitation source for the elastic wave propagation in the substrate. A resonator die has very rough sidewalls, because it is created by cutting a whole silicon wafer into many dies using a dicing saw. Similar to mirror reflection, the rough sidewalls will absorb the elastic waves and result in no energy being reflected back to the substrate. Hence, it is reasonable to assume that all the vibration energy of a micromechanical resonator that enters its substrate propagates away to large distances, so that no energy is returned to the resonator. To make the theoretical derivation of the vibration displacement on substrate possible [16–20], it is also assumed that the stress is uniformly distributed across a clamped region.

In order to calculate support loss, the assumptions discussed above are summarized as below:

(1) There is negligible coupling between the vibrations in the resonator and the elastic waves in the substrate [12,15,21].
(2) All the vibration energy entering the substrate is carried away to infinity and therefore is considered to be lost [12,15,21].
(3) The time-harmonic stress is uniformly distributed across a clamped region [12,15–20].

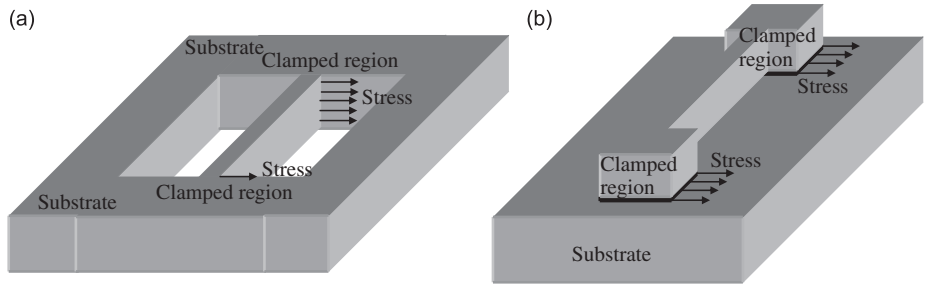

Fig. 3. Two typical configurations of a micromechanical resonator with respect to its substrate (note: the ratio of the resonator and the substrate is out of proportion for better illustration), (a) a resonator is located within a substrate, where time-harmonic stress sources are located within the substrate and (b) a resonator sits on top of a substrate, where time-harmonic stress sources are on the surface of the substrate.

Consequently, the vibrations of a micromechanical resonator can be described using the classic vibration theory, where the clamped region has no displacement but suffers a time-harmonic stress from the vibrations. The substrate is modeled as either a semi-infinite or infinite elastic medium, giving rise to the vibration displacement on substrate caused by the stress source. Then, support loss in a micromechanical resonator can be formulated as the integral of the product of the stress and the vibration displacement across the clamped region per cycle of vibration [12]:

$$\Delta W = \pi \int_{\text{clamped region}} \text{stress} \cdot \text{displacement}. \tag{2}$$

In this equation, stress and displacement denote the amplitudes of the two time-harmonic parameters, since π is factored in to account for the time-harmonic nature of the vibrations and elastic waves.

2.2. Two typical configurations of a micromechanical resonator with respect to its substrate

Figs. 3(a) and (b) illustrate two typical configurations of a micromechanical resonator with respect to its substrate: a resonator is located within its substrate and a resonator sits on top of its substrate, respectively. For simplicity, their integrated transducers for operation are not illustrated here. As shown in Fig. 3, a micromechanical resonator is fixed to its substrate through the clamped regions. Each clamped region serves as a time-harmonic stress source to excite elastic waves into the substrate. Based on these two typical configurations, the time-harmonic stress sources can be categorized into two groups:

(1) Time-harmonic stress sources located within a substrate.
(2) Time-harmonic stress sources located on the surface of a substrate.

In addition, depending on the resonant mode utilized, a time-harmonic stress source can be either shear stress or normal stress, but, in general, not both at the same time. The effect of bending moment on support loss is negligible [12,21] relative to that caused by shear stress or normal stress and therefore is not considered here. Furthermore, a micromechanical resonator may have either single stress source or multiple stress sources, depending on how many clamped regions it has. The following three sections will derive the mathematical expressions for the vibration displacement on substrate under several typical time-harmonic stress sources in micromechanical resonators.

3. Vibration displacement due to time-harmonic stress sources located within a substrate

The typical time-harmonic stress sources located within a substrate are illustrated in Figs. 4 and 5. The substrate is assumed as either semi-infinite or infinite thin-plate medium [12] of thickness, h, and the elastic wave propagation can be described using the two-dimensional (2D) elastic wave theory. Therefore, this section

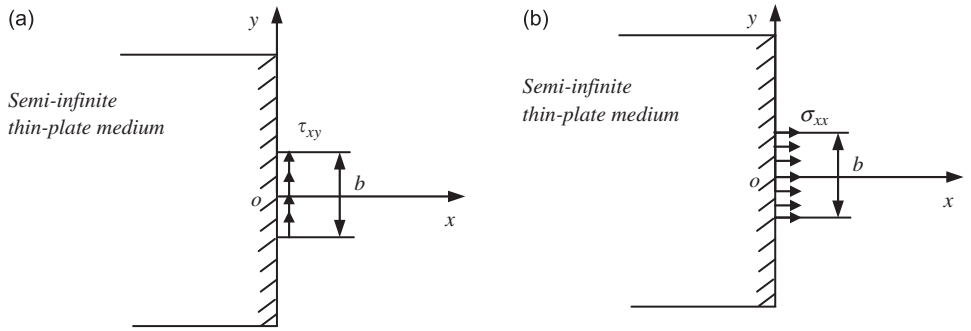

Fig. 4. Single time-harmonic stress source is applied on a semi-infinite thin-plate medium of thickness, h, (a) shear stress source and (b) normal stress source.

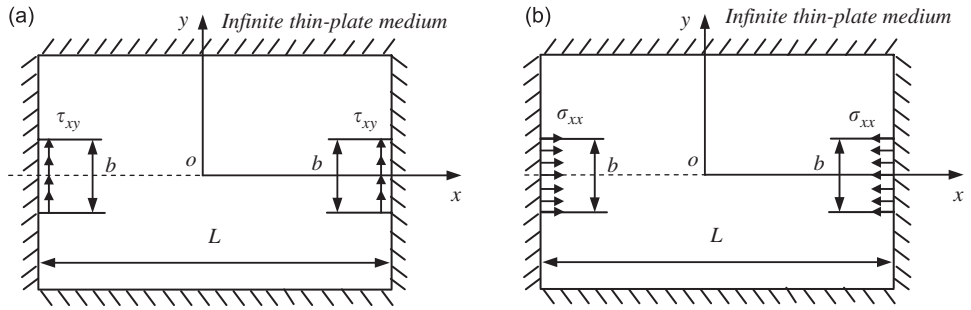

Fig. 5. Double time-harmonic stress sources are applied on an infinite thin-plate medium of thickness, h, (a) shear stress sources and (b) normal stress sources.

first briefly reviews the 2D elastic wave equations and their Fourier transform and then combine the elastic wave equations with different time-harmonic stress sources for obtaining the mathematical expressions for the average vibration displacement on substrate.

3.1. 2D elastic wave equations and their Fourier transform

The governing equations for the 2D elastic wave theory with in-plane (x–y plane) displacements are given by Ref. [22]:

$$\frac{\partial^2 u_x}{\partial t^2} = c_L^2 \frac{\partial^2 u_x}{\partial x^2} + c_T^2 \frac{\partial^2 u_x}{\partial y^2} + (c_L^2 - c_T^2)\frac{\partial^2 u_y}{\partial x \partial y}, \tag{3a}$$

$$\frac{\partial^2 u_y}{\partial t^2} = c_L^2 \frac{\partial^2 u_y}{\partial y^2} + c_T^2 \frac{\partial^2 u_y}{\partial x^2} + (c_L^2 - c_T^2)\frac{\partial^2 u_x}{\partial x \partial y}, \tag{3b}$$

where u_x and u_y are the displacement along the x-axis and y-axis, respectively. The 2D elastic waves can be separated into longitudinal and transverse waves with propagation velocities:

$$c_L^2 = \frac{E}{\rho(1-\upsilon^2)} \quad \text{and} \quad c_T^2 = \frac{E}{2\rho(1+\upsilon)}, \tag{4}$$

where c_L and c_T are the propagation velocities for longitudinal and transverse waves in the thin-plate (2D) medium, respectively; ρ is the density of substrate material; E and υ are the Young's modulus and the Poisson's ratio of the substrate material, respectively. The ratio of the longitudinal propagation velocity to the

transverse propagation velocity is denoted by:

$$\gamma = c_L/c_T = \sqrt{\frac{2}{1-\upsilon}}. \tag{5}$$

Due to the time-harmonic nature of the elastic waves, the following relations exist:

$$u_x = u\mathrm{e}^{\mathrm{i}\omega t} \quad \text{and} \quad u_y = v\mathrm{e}^{\mathrm{i}\omega t}, \tag{6}$$

where ω denotes the frequency of the elastic waves; u and v denote the elastic wave amplitudes along the x-axis and the y-axis, respectively. We further assume the following definitions [17]:

$$\Delta = \frac{\partial u}{\partial x} + \frac{\partial v}{\partial y} \quad \text{and} \quad \Omega = \frac{\partial u}{\partial y} - \frac{\partial v}{\partial x}. \tag{7}$$

Then, Eq. (2) can be rewritten as [17]:

$$-\omega^2 u = c_L^2 \frac{\partial \Delta}{\partial x} + c_T^2 \frac{\partial \Omega}{\partial y}, \tag{8a}$$

$$-\omega^2 v = c_L^2 \frac{\partial \Delta}{\partial y} - c_T^2 \frac{\partial \Omega}{\partial x}. \tag{8b}$$

The above two equations can be further reorganized as [17]:

$$c_L^2\left(\frac{\partial^2 \Delta}{\partial x^2} + \frac{\partial^2 \Delta}{\partial y^2}\right) + \omega^2 \Delta = 0, \tag{9a}$$

$$c_T^2\left(\frac{\partial^2 \Omega}{\partial x^2} + \frac{\partial^2 \Omega}{\partial y^2}\right) + \omega^2 \Omega = 0. \tag{9b}$$

Due to the geometrical infinity of the substrate, the variable, x, needs to be removed from the above equations. For this reason, we use the Fourier transform and its inverse transform defined by the following equations [23]:

$$g(\xi) = \int_{-\infty}^{+\infty} f(x)\mathrm{e}^{-\mathrm{i}\xi y}\,\mathrm{d}y, \tag{10a}$$

$$f(y) = \frac{1}{2\pi}\int_{-\infty}^{+\infty} g(\xi)\mathrm{e}^{\mathrm{i}\xi y}\,\mathrm{d}\xi, \tag{10b}$$

where ξ is the variable of the Fourier transform. By applying the Fourier transform to Eqs. (8) and (9), the 2D elastic wave equations can be rewritten in the following format [17]:

$$-\omega^2 u_F = c_L^2 \frac{\mathrm{d}\Delta_F}{\mathrm{d}x} + \mathrm{i}\xi c_T^2 \Omega_F, \tag{11a}$$

$$-\omega^2 v_F = c_L^2 \mathrm{i}\xi \Delta_F - c_T^2 \frac{\mathrm{d}\Omega_F}{\mathrm{d}x}, \tag{11b}$$

$$\frac{\mathrm{d}^2 \Delta_F}{\mathrm{d}x^2} - \left(\xi^2 - \frac{\omega^2}{c_L^2}\right)\Delta_F = 0, \tag{12a}$$

$$\frac{\mathrm{d}^2 \Omega_F}{\mathrm{d}x^2} - \left(\xi^2 - \frac{\omega^2}{c_T^2}\right)\Omega_F = 0, \tag{12b}$$

where the subscript F denotes the Fourier transform.

3.2. Time-harmonic stresses and their Fourier transform

The excitation sources for the elastic wave propagation in a substrate are the time-harmonic stress sources located at the clamped regions of a micromechanical resonator. In terms of in-plane displacements in a thin-plate medium, the shear stress toward the y-axis and the normal stress toward the x-axis, as illustrated in Figs. 4 and 5, are given by Ref. [22]:

$$\tau_{xy} = \frac{E}{2(1+\upsilon)}\left(\frac{\partial u}{\partial y} + \frac{\partial v}{\partial x}\right), \tag{13a}$$

$$\sigma_{xx} = \frac{E}{1-\upsilon^2}\left(\frac{\partial u}{\partial x} + \upsilon\frac{\partial v}{\partial y}\right), \tag{13b}$$

respectively, which can also be rewritten as [17]:

$$\frac{\omega^2}{\rho c_T^4}\tau_{xy} = \left[\frac{\partial^2 \Omega}{\partial x^2} - \frac{\partial^2 \Omega}{\partial y^2}\right] - 2\gamma^2\frac{\partial^2 \Delta}{\partial x \partial y}, \tag{14a}$$

$$\frac{\omega^2}{\rho c_T^4}\sigma_{xx} = -2\frac{\partial^2 \Omega}{\partial x \partial y} - \gamma^4\frac{\partial^2 \Delta}{\partial x^2} + (2\gamma^2 - \gamma^4)\frac{\partial^2 \Delta}{\partial y^2}. \tag{14b}$$

Taking the Fourier transform of Eqs. (14) yields the following expressions for the transformed excitation stress sources [17]:

$$\frac{\omega^2}{\rho c_T^4}\tau_{xy_F} = \left[\frac{\mathrm{d}^2 \Omega_F}{\mathrm{d}x^2} + \xi^2 \Omega_F\right] - 2\mathrm{i}\xi\gamma^2\frac{\mathrm{d}\Delta_F}{\mathrm{d}x}, \tag{15a}$$

$$\frac{\omega^2}{\rho c_T^4}\sigma_{xx_F} = -2\mathrm{i}\xi\frac{\mathrm{d}\Omega_F}{\mathrm{d}x} - \gamma^4\frac{\mathrm{d}^2 \Delta_F}{\mathrm{d}x^2} - (2\gamma^2 - \gamma^4)\xi^2\Delta_F. \tag{15b}$$

3.3. Vibration displacement due to single time-harmonic stress source

As illustrated in Fig. 4(a), a uniform shear stress source is applied across the clamped region at the edge of the semi-infinite thin-plate medium:

$$\tau_{xy} = \tau_0, \quad \text{for } x = 0,\ y \in (-b/2, b/2), \tag{16}$$

where τ_0 is a constant and is determined by the vibrations in a micromechanical resonator.

Through combing Eq. (16) with Eqs. (10), (11), (12) and (15), the mathematical expression for the average vibration displacement across the clamped region is written as [17]:

$$v = b\tau_0\left\{\frac{4}{\pi}\frac{1+\upsilon}{E(1-\upsilon)}\Pi_1\right\} \quad \text{for } x = 0,\ y \in (-b/2, b/2), \tag{17}$$

where

$$\Pi_1(\gamma) = \mathrm{Im}\left(\int_0^\infty \frac{\sqrt{\zeta^2 - \gamma^2}}{F_0(\zeta)}\,\mathrm{d}\zeta\right)$$

is the imaginary part of the integral constant in the parenthesis. In this integral, $\zeta = \xi c_L/\omega$ is assumed and the following relation is utilized:

$$F_0(\zeta, \gamma) = \{2\zeta^2 - \gamma^2\}^2 - 4\zeta^2\sqrt{\zeta^2 - \gamma^2}\sqrt{\zeta^2 - 1}. \tag{18}$$

As illustrated in Fig. 4(b), a uniform normal stress source is applied across the clamped region at the edge of the semi-infinite thin-plate medium:

$$\sigma_{xx} = \sigma_0 \quad \text{for } x = 0,\ y \in (-b/2, b/2), \tag{19}$$

where σ_0 is a constant and is determined by the vibrations in a micromechanical resonator.

Similarly, the combination of Eq. (19) with Eqs. (10)–(12) and (15) gives rise to the average vibration displacement across the clamped region [17]:

$$u = b\sigma_0 \left\{ \frac{4}{\pi} \frac{1+\upsilon}{E(1-\upsilon)} \Pi_2 \right\} \quad \text{for } x = 0,\ y \in (-b/2, b/2), \tag{20}$$

where

$$\Pi_2(\gamma) = \mathrm{Im}\left(\int_0^\infty \frac{\sqrt{\zeta^2 - 1}}{F_0(\zeta)} \mathrm{d}\zeta \right).$$

3.4. Vibration displacement due to double time-harmonic stress sources

As illustrated in Fig. 5, this subsection considers the case where double time-harmonic stress sources are applied across the two rectangular clamped regions, with a distance of L between the centers of the two regions, on an infinite thin-plate elastic medium. To account for the effect of the two stress sources on the vibration displacement, first, we need to analyze the vibration displacement across each clamped region caused by only one stress source. Then, the vibration displacement across each clamped region caused by the other stress source is added up, according to the superposition principle.

As illustrated in Fig. 5(a), there are two identical uniform shear stress sources, τ_0, across the two rectangular clamped regions:

$$\tau_{xy} = \tau_0 \quad \text{for } x = \pm L/2,\ y \in (-b/2, b/2). \tag{21}$$

Now, we consider only the stress source at $x = -L/2$. By combining this stress source with Eqs. (10)–(12) and (15), the average vibration displacements across the two clamped regions, under the stress source at $x = -L/2$, take the following format:

$$v = \frac{b\tau_0}{8E}(\upsilon + 1)(\upsilon - 3) \quad \text{for } x = -L/2,\ y \in (-b/2, b/2), \tag{22a}$$

$$v = \frac{b\tau_0}{2\pi E} \Pi_3 \quad \text{for } x = L/2,\ y \in (-b/2, b/2), \tag{22b}$$

where

$$\Pi_3(\gamma, k) = \int_0^1 \left[\frac{\zeta^2}{\sqrt{1-\zeta^2}} \cos\left(\sqrt{1-\zeta^2} 2\pi k \right) (1-\upsilon^2) + 2(1+\upsilon)\sqrt{1-\zeta^2} \cos\left(\sqrt{1-\zeta^2} 2\pi k \right) \right] \mathrm{d}\zeta$$

is an integral constant having a pure real value. Note that the distance between the centers of the two stress sources is expressed in terms of a dimensionless parameter—wavenumber, $k = L/\lambda$, where $\lambda = C_L/f$ denotes the wavelength in the substrate, with f being the resonant frequency of the elastic waves and also that of the elastic vibrations of the resonator.

According to the superposition principle, the average vibration displacement across each clamped region, under the two stress sources, has the same expression written as below:

$$v = \frac{b\tau_0}{8E}(\upsilon + 1)(\upsilon - 3) + \frac{b\tau_0}{2\pi E} \Pi_3 \quad \text{for } x = \pm L/2,\ y \in (-b/2, b/2). \tag{23}$$

As illustrated in Fig. 5(b), there are two identical uniform normal stress sources, σ_0, across the two rectangular clamped regions:

$$\sigma_{xx} = \sigma_0 \quad \text{for } x = \pm L/2,\ y \in (-b/2, b/2). \tag{24}$$

Similarly, we first obtain the expressions for the average vibration displacement, under the stress source at $x=-L/2$, across the two clamped regions:

$$u=\frac{b\sigma_0}{8E}(\upsilon+1)(\upsilon-3) \quad \text{for } x=L/2,\ y\in(-b/2,b/2), \tag{25a}$$

$$u=\frac{b\sigma_0}{2\pi E}\Pi_4 \quad \text{for } x=L/2,\ y\in(-b/2,b/2), \tag{25b}$$

where

$$\Pi_4(\gamma,k)=\int_0^1\left[\frac{\zeta^2}{\sqrt{1-\zeta^2}}\cos\left(\sqrt{1-\zeta^2}2\pi k\right)2(1+\upsilon)+(1-\upsilon^2)\sqrt{1-\zeta^2}\cos\left(\sqrt{1-\zeta^2}2\pi k\right)\right]\mathrm{d}\zeta$$

is an integral constant having a pure real value. Then, based on the superposition principle, the average displacement across each clamped region, under the two stress sources, takes the following format:

$$u=\frac{b\sigma_0}{8E}(\upsilon+1)(\upsilon-3)+\frac{b\sigma_0}{2\pi E}\Pi_4 \quad \text{for } x=\pm L/2,\ y\in(-b/2,b/2). \tag{26}$$

4. Vibration displacement due to single circular time-harmonic stress source located on the surface of a substrate

As illustrated in Fig. 6, a uniform normal stress source is applied across the circular clamped region of radius, a, on the surface of the substrate and excites the elastic wave propagation into the substrate. In this case, the substrate is modeled as a semi-infinite elastic medium and the cylindrical coordinates (r, θ, z) are utilized accordingly. Since all the variables involved are independent of the circumferential direction, θ, the terms related to this direction are omitted in the following analysis. This section reviews the 3D elastic wave equations in cylindrical coordinates and their Hankel transform, and combines the elastic wave equations with the stress source to obtain the average vibration displacement on substrate.

4.1. 3D elastic wave equations and their Hankel transform

As illustrated in Fig. 6, the substrate is modeled as a semi-infinite medium and its behavior can be described using the 3D elastic wave theory [17]:

$$\frac{\partial^2\Omega}{\partial z^2}+\frac{\partial}{\partial r}\left[\frac{1}{r}\frac{\partial(r\Omega)}{\partial r}\right]+\frac{\omega^2}{c_T^2}\Omega=0, \tag{27a}$$

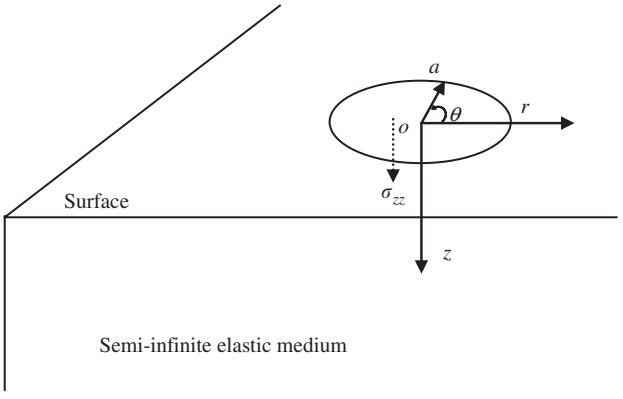

Fig. 6. A circular time-harmonic stress source is applied on the surface of a semi-infinite elastic medium.

$$\frac{\partial^2 \Delta}{\partial z^2} + \frac{1}{r}\frac{\partial}{\partial r}\left[r\frac{\partial \Delta}{\partial r}\right] + \frac{\omega^2}{c_L^2}\Delta = 0. \tag{27b}$$

In the above equations, it has assumed that $\vec{u}(r,z,t) = e^{i\omega t}(u_r\vec{r} + u_z\vec{z})$, where ω is the frequency of the elastic waves; u_r and u_z are the elastic wave amplitudes along the r-axis and z-axis, respectively. In addition, the following relations are defined [17]:

$$\Delta = \frac{1}{r}\frac{\partial}{\partial r}(ru_r) + \frac{\partial u_z}{\partial z} \quad \text{and} \quad \Omega = \frac{\partial u_r}{\partial z} - \frac{\partial u_z}{\partial r}. \tag{28}$$

The propagation velocities for the longitudinal wave, c_L, and the transverse wave, c_T, in a 3D elastic medium are, respectively, given by Ref. [17]:

$$c_L^2 = \frac{E(1-\upsilon)}{\rho(1+\upsilon)(1-2\upsilon)}, \quad c_T^2 = \frac{E}{2\rho(1+\upsilon)}. \tag{29}$$

Again, $\gamma = c_L/c_T$ is defined as the ratio of the longitudinal wave propagation velocity to the transverse wave propagation velocity:

$$\gamma = c_L/c_T = \sqrt{\frac{2(1-\upsilon)}{1-2\upsilon}}. \tag{30}$$

To account for the geometrical infinity of the substrate and cylindrical coordinates, we use the Hankel transform defined by the following expressions [23]:

$$g(\xi)_{H0} = \int_0^\infty f(r) r J_0(\xi r)\,\mathrm{d}r, \quad g(\xi)_{H1} = \int_0^\infty f(r) r J_1(\xi r)\,\mathrm{d}r, \tag{31a}$$

$$f(r)_{H0} = \int_0^\infty g(\xi)\xi J_0(\xi r)\,\mathrm{d}r, \quad f(r)_{H1} = \int_0^\infty g(\xi)\xi J_1(\xi r)\,\mathrm{d}r, \tag{31b}$$

where ξ is the variable of this transform. Applying the Hankel transform to Eqs. (27) and (28) leads to the following relations:

$$u_{rH1} = -\frac{c_T^2}{\omega^2}\left[\frac{\mathrm{d}\Omega_{H1}}{\mathrm{d}z} - \xi\gamma^2\Delta_{H0}\right], \tag{32a}$$

$$u_{zH0} = -\frac{c_T^2}{\omega^2}\left[\gamma^2\frac{\mathrm{d}\Delta_{H0}}{\mathrm{d}z} - \xi\Omega_{H1}\right], \tag{32b}$$

$$\frac{\mathrm{d}^2\Omega_{H1}}{\mathrm{d}z^2} - \left(\xi^2 - \frac{\omega^2}{c_T^2}\right)\Omega_{H1} = 0, \tag{33a}$$

$$\frac{\mathrm{d}^2\Delta_{H0}}{\mathrm{d}z^2} - \left(\xi^2 - \frac{\omega^2}{c_L^2}\right)\Delta_{H0} = 0, \tag{33b}$$

where subscripts $H0$ and $H1$ denote the Hankel transform.

4.2. Time-harmonic stresses and their Hankel transform

In terms of the displacements in the substrate, the normal stress along the z-axis, σ_{zz}, and the shear stress along the r-axis, τ_{zr}, are written as below [17]:

$$\frac{\omega^2}{\rho c_t^4}\sigma_{zz} = \frac{2}{r}\frac{\partial}{\partial r}\left(r\frac{\partial\Omega}{\partial z}\right) - \gamma^4\frac{\partial^2\Delta}{\partial z^2} - \frac{\gamma^2(\gamma^2-2)}{r}\frac{\partial}{\partial r}\left(r\frac{\partial\Delta}{\partial r}\right), \tag{34a}$$

$$\frac{\omega^2}{\rho c_t^4}\tau_{zr} = \frac{\partial}{\partial r}\left(\frac{1}{r}\frac{\partial(r\Omega)}{\partial r}\right) - \frac{\partial^2\Omega}{\partial z^2} - 2\gamma^2\frac{\partial^2\Delta}{\partial r\partial z}. \tag{34b}$$

The Hankel transform of the above equations gives rise to the following relations [17]:

$$\frac{\omega^2}{\rho c_T^4}\sigma_{zzH0} = 2\xi\frac{\mathrm{d}\Omega_{H1}}{\mathrm{d}z} - \gamma^4\frac{\mathrm{d}^2\Delta_{H0}}{\mathrm{d}z^2} + \gamma^2(\gamma^2-2)\xi^2\Delta_{H0}, \tag{35a}$$

$$\frac{\omega^2}{\rho c_T^4}\tau_{zrH1} = -\xi^2\Omega_{H1} - \frac{\mathrm{d}^2\Omega_{H1}}{\mathrm{d}z^2} + 2\gamma^2\xi\frac{\mathrm{d}\Delta_{H0}}{\mathrm{d}z}. \tag{35b}$$

4.3. Vibration displacement due to single normal stress source

As illustrated in Fig. 6, the normal stress source over the clamped region on the substrate is expressed as below:

$$\sigma_{zz} = \sigma_0 \quad \text{for } z=0,\ r\leqslant a, \tag{36}$$

where σ_0 is a constant and is determined by the vibrations in a micromechanical resonator.

Finally, combining Eq. (36) with Eqs. (31)–(33) and (35) leads to the average vibration displacement across the clamped region [17]:

$$u_z = \sigma_0 a^2\frac{c_L\omega}{2\rho c_T^4}\Pi_5 \quad \text{for } z=0,\ r\leqslant a, \tag{37}$$

where

$$\Pi_5(\gamma) = \mathrm{Im}\left(\int_0^\infty \frac{\sqrt{\zeta^2-1}}{F_0(\zeta)}\zeta\,\mathrm{d}\zeta\right),$$

with ζ and $F_0(\zeta)$ being the same as defined in the previous section.

5. Vibration displacement due to rectangular time-harmonic stress sources on the surface of a substrate

As illustrated in Figs. 7 and 8, rectangular time-harmonic stress sources on the surface of a substrate are considered here and the rectangular coordinates are utilized accordingly. This section reviews the 3D elastic wave equations in rectangular coordinates and their double Fourier transform, and combines the elastic wave equations with the rectangular stress sources to obtain the expressions for the average vibration displacement on substrate.

5.1. 3D elastic wave equations and their double Fourier transform

The substrate is modeled as a semi-infinite elastic medium and its behavior can be described by the 3D elastic wave theory, expressed as below [19,20]:

$$(c_L^2 - c_T^2)\nabla(\Delta) + c_T^2\nabla^2\vec{u} = -\omega^2\vec{u}, \tag{38}$$

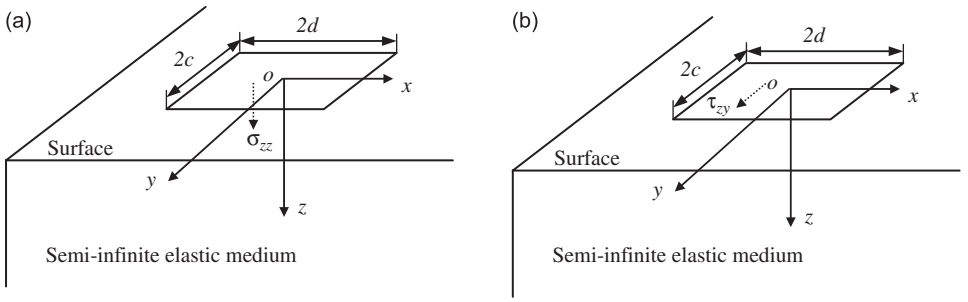

Fig. 7. Single rectangular time-harmonic load is applied on the surface of a semi-infinite elastic medium (a) single normal stress source and (b) single shear stress source.

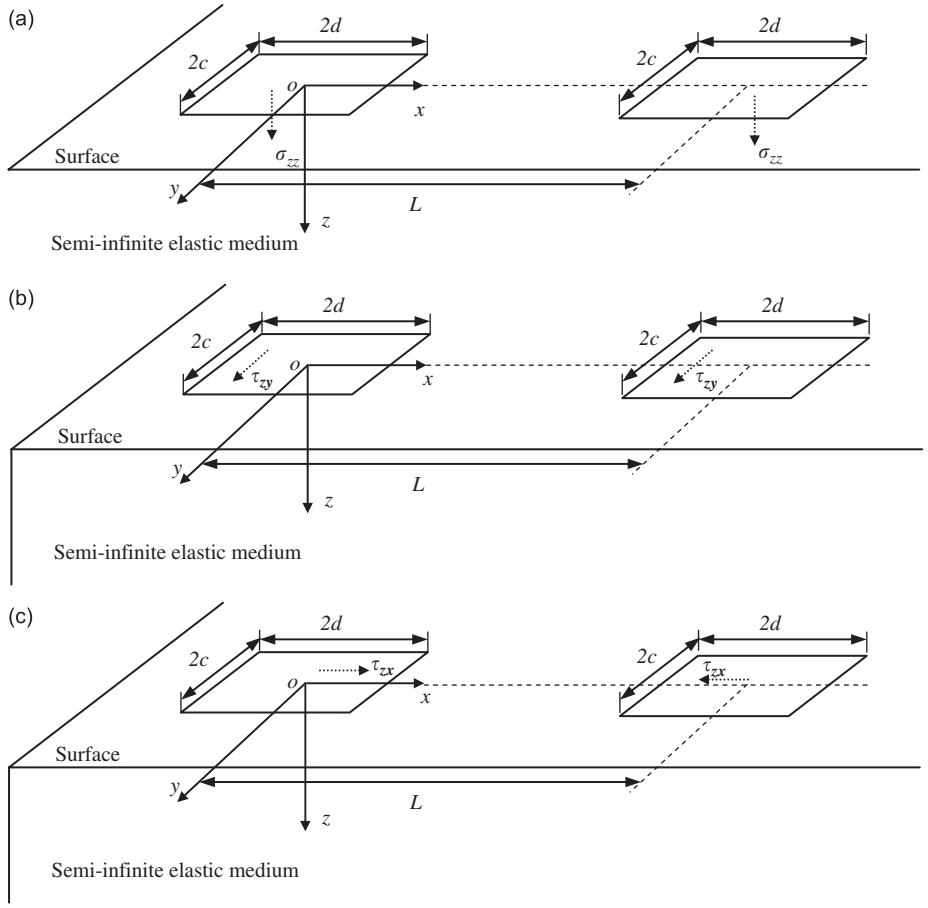

Fig. 8. Double time-harmonic loads are applied on the surface of a semi-infinite elastic medium (a) double normal stress sources (b) double shear stress sources in parallel and (c) double shear stress sources in the opposite directions.

where $\vec{u}$ represents the vector of the elastic wave amplitudes, having components, (u, v, w) along the three axes. Taking the same expressions as Eq. (29), c_L and c_T are the propagation velocities of longitudinal and transverse elastic waves, respectively. The elastic dilatation, Δ, is expressed by:

$$\Delta = \frac{\partial u}{\partial x} + \frac{\partial v}{\partial y} + \frac{\partial w}{\partial z}. \tag{39}$$

Taking the divergence of Eq. (38) and dividing it by ρ gives rise to the following relation [19,20]:

$$\left(\nabla^2 + \frac{\omega^2}{c_L^2}\right)\Delta = 0. \tag{40}$$

To account for the geometrical infinity along both the x-axis and the y-axis, we use the double Fourier transform and its inverse transform defined as below [23]:

$$g(\eta, \xi, z) = \int_{-\infty}^{\infty}\int_{-\infty}^{\infty} f(x, y, z)\, \mathrm{e}^{\mathrm{i}(\eta x + \xi y)}\, \mathrm{d}\eta\, \mathrm{d}\xi, \tag{41a}$$

$$f(x, y, z) = \frac{1}{4\pi^2}\int_{-\infty}^{\infty}\int_{-\infty}^{\infty} g(\xi, \eta, z)\, \mathrm{e}^{-\mathrm{i}(\eta x + \xi y)}\, \mathrm{d}x\, \mathrm{d}y, \tag{41b}$$

where η and ξ are the variables for this transform. Taking the double Fourier transform of Eqs. (38) and (40) yields the following relations:

$$\frac{\partial^2 \vec{u}_F}{\partial z^2} - \beta^2 \vec{u}_F + (\gamma^2 - 1)\left(\frac{\partial \Delta_F}{\partial z}\vec{k} - \mathrm{i}\eta\Delta_F \vec{i} - \mathrm{i}\xi \Delta_F \vec{j}\right) = 0, \tag{42}$$

$$\frac{\partial^2 \Delta_F}{\partial z^2} = \alpha^2 \Delta_F, \tag{43}$$

where $\alpha = \sqrt{\eta^2 + \xi^2 - \omega^2/c_L^2}$ and $\beta = \sqrt{\eta^2 + \xi^2 - \omega^2/c_T^2}$; $\vec{i}, \vec{j}, \vec{k}$ denote the unit vectors along the three axes; and the subscript F denotes the double Fourier transform.

5.2. Time-harmonic stresses and their double Fourier transform

In terms of the displacements in the substrate, the time-harmonic stresses along the three axes can be written as [19,20]:

$$\tau_{zx} = \rho c_T^2 \left(\frac{\partial u}{\partial z} + \frac{\partial w}{\partial x}\right), \tag{44a}$$

$$\tau_{zy} = \rho c_T^2 \left(\frac{\partial v}{\partial z} + \frac{\partial w}{\partial y}\right), \tag{44b}$$

$$\sigma_{zz} = \rho c_T^2 (\gamma^2 - 2)\Delta + 2\rho c_T^2 \frac{\partial w}{\partial z}. \tag{44c}$$

By taking the double Fourier transform of Eqs. (44), the following relations exist [19,20]:

$$\tau_{zx_F} = \rho c_T^2 \left(\frac{\partial u_F}{\partial z} - \mathrm{i}\eta w_F\right), \tag{45a}$$

$$\tau_{zy_F} = \rho c_T^2 \left(\frac{\partial v}{\partial z} - \mathrm{i}\xi w_F\right), \tag{45b}$$

$$\sigma_{zz_F} = \mathrm{i}\rho c_T^2 (2 - \gamma^2)(\eta u_F + \xi v_F) + \rho c_L^2 \frac{\partial w_F}{\partial z}. \tag{45c}$$

5.3. Vibration displacement due to single time-harmonic stress source

This subsection focuses on deriving the vibration displacement caused by single time-harmonic stress source. As illustrated In Fig. 7(a), a uniform normal stress source, σ_{zzo}, is applied across the rectangular stress source on the substrate. Then, the average vibration displacement across the rectangular clamped region located at $z = 0$, $x \in (-d, d)$ and $y \in (-c, c)$ is written as [19,20]:

$$w = \frac{\sigma_{zzo}}{\pi^3} \frac{dc\omega\gamma}{2\rho c_T^3} \Pi_6 \quad \text{for } z = 0,\ x(-d, d),\ y(-c, c), \tag{46}$$

where

$$\Pi_6(\gamma) = \mathrm{Im}\left(\int_{-\infty}^{\infty}\int_{-\infty}^{\infty} \frac{\sqrt{\varsigma^2 - 1}}{(\gamma^2 - 2\varsigma^2)^2 - 4\varsigma^2\sqrt{\varsigma^2 - \gamma^2}\sqrt{\varsigma^2 - 1}}\, \mathrm{d}\zeta\, \mathrm{d}\vartheta\right)$$

is the imaginary part of the integral constant in the parenthesis; and $\zeta = (c_L/\omega)\eta$, $\vartheta = (c_L/\omega)\xi$, $\varsigma = \sqrt{\zeta^2 + \vartheta^2}$.

As illustrated in Fig. 7(b), a uniform shear stress source, τ_{zyo}, along the y-axis is located at the rectangular clamped region. Then, the average vibration displacement across the rectangular clamped region located at

$z=0$, $x\in(-d,\,d)$ and $y\in(-c,\,c)$ can be expressed as:

$$v=\frac{\tau_{zyo}}{\pi^3}\frac{\mathrm{d}c\omega}{2\rho c_T^3\gamma}\Pi_7 \quad \text{for } z=0,\ x(-d,d),\ y(-c,c), \tag{47}$$

where

$$\Pi_7(\gamma)=\mathrm{Im}\left(\int_{-\infty}^{\infty}\int_{-\infty}^{\infty}\frac{(\vartheta^2+2\zeta^2-\gamma^2)(2\zeta^2-\gamma^2)-4\zeta^2\sqrt{\zeta^2+\vartheta^2-1}\sqrt{\zeta^2+\vartheta^2-\gamma^2}+2\zeta^2\vartheta^2}{4(\zeta^2+\vartheta^2-\gamma^2)(\zeta^2+\vartheta^2)\sqrt{\zeta^2+\vartheta^2-1}-(2(\zeta^2+\vartheta^2)-\gamma^2)^2\sqrt{\zeta^2+\vartheta^2-\gamma^2}}\,\mathrm{d}\zeta\,\mathrm{d}\vartheta\right)$$

with $\zeta=(c_L/\omega)\eta$ and $\vartheta=(c_L/\omega)\xi$.

5.4. Vibration displacement due to double time-harmonic stress sources

As illustrated in Fig. 8, two uniform time-harmonic stress sources are simultaneously applied across the two rectangular clamped regions, with a distance of L between the centers of the two regions on the surface of a substrate. In order to obtain the mathematical expressions for the vibration displacement in this case, this section directly utilizes the obtained results in the previous subsection, based on the superposition principle.

Fig. 8(a) illustrates two identical uniform normal stress sources, σ_{zzo}, located at the two rectangular clamped regions. Therefore, based on the superposition principle and Eq. (46), the average vibration displacement across each clamped region, under the two stress sources, is written as below:

$$w=\frac{-\sigma_{zzo}}{\pi^3}\frac{dc\omega\gamma}{2\rho c_T^3}\Pi_8 \quad \text{for } \left|\begin{array}{l} z=0,\ x(-d,d),\ y(-c,c)\\ z=0,\ x(L-d,L+d),\ y(-c,c)\end{array}\right., \tag{48}$$

where

$$\Pi_8(\gamma,k)=\mathrm{Im}\left(\int_{-\infty}^{\infty}\int_{-\infty}^{\infty}\frac{\sqrt{\varsigma^2-1}}{(\gamma^2-2\varsigma^2)^2-4\varsigma^2\sqrt{\varsigma^2-\gamma^2}\sqrt{\varsigma^2-1}}[1+\cos(2\pi k\gamma\zeta)]\,\mathrm{d}\zeta\,\mathrm{d}\vartheta\right),$$

with ζ, ϑ, and ς are the same as defined in Π_6.

As illustrated in Fig. 8(b), we consider the case where two identical uniform shear stress sources along the y-axis are applied on the surface of a substrate. Based on the superposition principle and Eq. (47), the average vibration displacement across each clamped region, under the two stress sources, is written as below:

$$v=\frac{\tau_{zyo}}{\pi^3}\frac{dc\omega}{2\rho c_T^3\gamma}\Pi_9 \quad \text{for } \left|\begin{array}{l} z=0,\ x(-d,d),\ y(-c,c)\\ z=0,\ x(L-d,L+d),\ y(-c,c)\end{array}\right., \tag{49}$$

where

$$\Pi_9(\gamma,k)=\mathrm{Im}\left(\int_{-\infty}^{\infty}\int_{-\infty}^{\infty}\frac{(\vartheta^2+2\zeta^2-\gamma^2)(\gamma^2-2\zeta^2)+4\zeta^2\sqrt{\zeta^2+\vartheta^2-1}\sqrt{\zeta^2+\vartheta^2-\gamma^2}-2\zeta^2\vartheta^2}{(2(\zeta^2+\vartheta^2)-\gamma^2)^2\sqrt{\zeta^2+\vartheta^2-\gamma^2}-4(\zeta^2+\vartheta^2-\gamma^2)(\zeta^2+\vartheta^2)\sqrt{\zeta^2+\vartheta^2-1}}\right.$$
$$\left.\times[1+\cos(2\pi k\gamma\zeta)]\,\mathrm{d}\zeta\,\mathrm{d}\vartheta\right).$$

Fig. 8(c) illustrates two identical shear stress sources, τ_{zxo}, along the x-axis but in the opposite directions, at the two clamped rectangular regions on the surface of a substrate. Similarly, based on the superposition principle and Eq. (47), the average vibration displacement across each clamped region, under the two stress sources, is written as below:

$$u=\frac{\tau_{zxo}}{\pi^3}\frac{bc\omega}{2\rho c_T^3\gamma}\Pi_{10}, \tag{50}$$

where

$$\Pi_{10}(\gamma,k)=\mathrm{Im}\left(\int_{-\infty}^{\infty}\int_{-\infty}^{\infty}\frac{(\zeta^2+2\vartheta^2-\gamma^2)(\gamma^2-2\vartheta^2)+4\vartheta^2\sqrt{\zeta^2+\vartheta^2-1}\sqrt{\zeta^2+\vartheta^2-\gamma^2}-2\zeta^2\vartheta^2}{(2\zeta^2+2\vartheta^2-\gamma^2)^2\sqrt{\zeta^2+\vartheta^2-\gamma^2}-4\sqrt{\zeta^2+\vartheta^2-1}(\zeta^2+\vartheta^2-\gamma^2)(\zeta^2+\vartheta^2)}\cdot\right.$$
$$\left.\times[1-\cos(2\pi k\gamma\zeta)]\,\mathrm{d}\zeta\,\mathrm{d}\vartheta\right).$$

Note that the subtraction sign in the last term of the integrand is due to the opposite directions of the two stresses.

6. Discussion

Up to now, the mathematical expressions for the average vibration displacement on substrate, under those typical time-harmonic stress sources in micromechanical resonators, have been derived. These expressions are further summarized into Table 1 for the configuration of a resonator located within a substrate and Table 2 for the configuration of a resonator sitting on top of a substrate, respectively. It is worth mentioning that because the excitation sources for the elastic waves are from the vibrations of a micromechanical resonator, the frequency of the elastic waves is the same as the resonant frequency of the micromechanical resonator under study. The key design parameters of a resonator required for calculating the average vibration displacement on substrate are (1) the uniform stress amplitude on a clamped region, (2) the area of a clamped region, (3) resonant frequency, and (4) the distance of the centers of the two clamped regions for a resonator with two clamped regions, which has been previously expressed in terms of the dimensionless parameter, wave number (k).

Since stress sources are considered uniform and the derived vibration displacement is also the averaged value of the vibration displacement across a clamped/source region, support loss, Eq. (2), can be further simplified as below:

$$\Delta W=\pi\cdot\text{uniform stress}\cdot\text{average vibration displacement}\cdot\text{clamped region area}. \tag{51}$$

Based on this equation, the mathematical expressions for support loss in a micromechanical resonator are also included in Tables 1 and 2.

Table 1
Stress sources located within a substrate and their corresponding average vibration displacements across a clamped region.

Stress source	Average vibration displacement	Eq.	Support loss
Single shear stress source	$v=b\tau_0\left\{\frac{4}{\pi}\frac{1+\upsilon}{E(1-\upsilon)}\Pi_1(\gamma)\right\}$	(17)	$\Delta W=4b^2h\tau_0^2\left\{\frac{1+\upsilon}{E\cdot(1-\upsilon)}\Pi_1(\gamma)\right\}$
Single normal stress source	$u=b\sigma_0\left\{\frac{4}{\pi}\frac{1+\upsilon}{E(1-\upsilon)}\Pi_2(\gamma)\right\}$	(20)	$\Delta W=4b^2h\sigma_0^2\left\{\frac{1+\upsilon}{E(1-\upsilon)}\Pi_2(\gamma)\right\}$
Double shear stress sources	$v=\frac{b\tau_0}{8E}(\upsilon+1)(\upsilon-3)+\frac{b\tau_0}{2\pi E}\Pi_3(\gamma,k)$	(23)	$\Delta W=\pi b^2h\tau_0^2\left\{\frac{(\upsilon+1)(\upsilon-3)}{4E}+\frac{\Pi_3(\gamma,k)}{\pi E}\right\}$
Double normal stress sources	$u=\frac{b\sigma_0}{8E}(\upsilon+1)(\upsilon-3)+\frac{b\sigma_0}{2\pi E}\Pi_4(\gamma,k)$	(26)	$\Delta W=\pi b^2h\sigma_0^2\left\{\frac{(\upsilon+1)(\upsilon-3)}{4E}+\frac{\Pi_4(\gamma,k)}{\pi E}\right\}$

Table 2
Stress sources located on the surface of a substrate and their corresponding average vibration displacements across a clamped region (note: except that the first row denotes a circular stress source, all the rest denote rectangular stress sources.).

Stress source	Average vibration displacement	Eq.	Support loss
Single normal stress source (circular)	$u_z = \sigma_{zzo} a^2 \omega \frac{\gamma}{2\rho c_T^3} \Pi_5(\gamma)$	(37)	$\Delta W = \pi^2 \sigma_{zzo}^2 a^4 \omega \left\{ \frac{\gamma}{2\rho c_T^3} \Pi_5(\gamma) \right\}$
Single normal stress source	$w = \frac{\sigma_{zzo} dc\omega}{\pi^3} \frac{\gamma}{2\rho c_T^3} \Pi_6(\gamma)$	(46)	$\Delta W = \frac{2d^2 c^2 \sigma_{zzo}^2 \omega}{\pi^2} \left\{ \frac{\gamma}{\rho c_T^3} \Pi_6(\gamma) \right\}$
Single shear stress source	$v = \frac{\tau_{zyo} dc\omega}{\pi^3} \frac{1}{2\rho c_T^3 \gamma} \Pi_7(\gamma)$	(47)	$\Delta W = \frac{2d^2 c^2 \tau_{zyo}^2 \omega}{\pi^2} \left\{ \frac{1}{\rho c_T^3 \gamma} \Pi_7(\gamma) \right\}$
Double normal stress sources	$w = \frac{-\sigma_{zzo} dc\omega}{\pi^3} \frac{\gamma}{2\rho c_T^3} \Pi_8(\gamma, k)$	(48)	$\Delta W = \frac{-4d^2 c^2 \sigma_{zzo}^2 \omega}{\pi^2} \left\{ \frac{\gamma}{\rho c_T^3} \Pi_8(\gamma, \kappa) \right\}$
Double shear stress sources in parallel	$v = \frac{\tau_{zyo} dc\omega}{\pi^3} \frac{1}{2\rho c_T^3 \gamma} \Pi_9(\gamma, k)$	(49)	$\Delta W = \frac{4d^2 c^2 \tau_{zyo}^2 \omega}{\pi^2} \left\{ \frac{1}{\rho c_T^3 \gamma} \Pi_9(\gamma, k) \right\}$
Double shear stress sources in opposite	$u = \frac{\tau_{zxo} dc\omega}{\pi^3} \frac{1}{2\rho c_T^3 \gamma} \Pi_{10}(\gamma, k)$	(50)	$\Delta W = \frac{4d^2 c^2 \tau_{zxo}^2 \omega}{\pi^2} \left\{ \frac{1}{\rho c_T^3 \gamma} \Pi_{10}(\gamma, k) \right\}$

6.1. Support loss versus design parameters of a resonator and substrate materials

Based on the mathematical expressions for support loss listed in Tables 1 and 2, this subsection focuses on addressing the insights on the relation of support loss versus the key design parameters of a micromechanical resonator and substrate materials. As to support loss in a micromechanical resonator located within a substrate, the following insights have been observed, regardless of stress types and single or double stress sources:

(1) *Design parameters of a micromechanical resonator:* Support loss is linearly proportional to the squared stress, and the squared width of the clamped region. At the same time, support loss is proportional to the thickness of the resonator. Interestingly, support loss in a resonator with single clamped region is independent of the resonant frequency, while support loss in a resonator with two clamped regions is not related to the resonant frequency explicitly, but depends on the wavenumber of the distance between the centers of the two clamped regions.
(2) *Material properties of the substrate*: Support loss is linearly proportional to the reciprocal of the Young's modulus of the substrate material. This indicates that the stiffer the substrate material is, the less support loss is. In addition, support loss is also related to the Poisson's ratio of the substrate material, because the elastic waves in the substrate propagate along both the x-axis and y-axis.

As to support loss in a micromechanical resonator sitting on top of a substrate, the following insights have been observed, regardless of stress types and single or double stress sources:

(1) *Design parameters of a micromechanical resonator:* Support loss is proportional to both the squared stress and the square of the clamped region area. At the same time, support loss is linearly proportional to the resonant frequency of the resonator. This explains the experimental observation [24] that, as to micromechanical disk resonators sitting on top of the same substrate, a micromechanical disk resonator with a large clamped region shows a smaller Q than the one of the same design with a small clamped region (the same resonant frequency and same stored maximum vibration energy in the resonators). Support loss

in a resonator with two clamped regions is closely related to the wavenumber of the distance of the centers of the two clamped regions.

(2) *Material properties of the substrate*: Support loss is linearly proportional to the term, $1/2\rho c_T^3\gamma$, for single and double shear stress sources and the term, $\gamma/2\rho c_T^3$, for single and double normal stress sources. This indicates that support loss is proportional to $E^{3/2}$ of the substrate material. Certainly, support loss is also related to the Poisson's ratio and density of the substrate material.

6.2. Numerical values for the imaginary parts of the integral constants related to different time-harmonic sources

Now, we consider the numerical values for the imaginary parts of the integral constants related to the expressions for the average vibration displacement on substrate. It should be noted that only the imaginary value of an integral constant will contribute to support loss, because it is out-of-phase with the time-harmonic stress. Here, we need to point out that the integrals, Π_3 and Π_4, are in fact the imaginary values of their original integrals, whose imaginary parts can be separated from their real parts. The numerical values for these integral constants can be calculated using mathematical software, such as Matlab.

As to single stress sources, the imaginary parts of the integral constants are solely the function of the Poisson's ratio of the substrate materials, and is completely independent of all the design parameters of a resonator. Consequently, Table 3 lists the numerical values for these imaginary parts corresponding to those several typical materials used in the MEMS fabrication technology, where the material properties of single crystal silicon (SCS) along both the $\langle 1\,0\,0\rangle$ and $\langle 1\,1\,0\rangle$ orientations are used [25,26]. As shown in Table 3, the numerical values for the imaginary parts of the integral constants decrease with the Poisson's ratio, except the case for the single shear stress source from a micromechanical resonator sitting on top of a substrate. However, the values for these imaginary parts do not vary much with the Poisson's ratio. Accordingly, the Young's modulus of the substrate plays a relatively important role in determining support loss.

As to double stress sources, the numerical values for the imaginary parts of the integral constants are correlated to the Poisson's ratio of the substrate material and the design dimensionless parameter of a resonator–the wavenumber, which is included in the cosine term in the integrals. Figs. 9 and 10 show the relation of the numerical values of the imaginary parts of the integral constants, Π_3 and Π_4, versus the wavenumber of the distance between the centers of the two stress sources within a substrate, respectively. It is clear from these figures that the distance between the two clamped regions can significantly affect the numerical values for the imaginary parts and consequently support loss. Figs. 11–13 illustrate the relation between the numerical values for the imaginary parts of the integral constants, Π_9, Π_{11}, and Π_{14}, and the distance (in terms of the wavenumber, k) between the centers of the two stress sources on top of a substrate, respectively. The Poisson's ratio used for all these figures is 0.064, which is taken from the $\langle 1\,1\,0\rangle$ orientation of SCS. As to the case of the two normal stress sources and two shear stress sources in parallel, the numerical values for the imaginary parts drop significantly as the distance increases within the first half wave length, and then becomes stable. On the contrary, as to the case of the two shear stress sources in the opposite directions, the numerical value for the imaginary part increases dramatically within the first half wavelength and then becomes stable.

Table 3
The numerical values for the imaginary parts of the integral constants related to single time- harmonic sources.

	Silicon $\langle 1\,1\,0\rangle$	Polydiamond	Polysilicon	Silicon nitride	Silicon $\langle 1\,0\,0\rangle$
Poissons'ratio (υ)	0.064	0.12	0.22	0.27	0.28
Young's Modulus (E, GPa)	169	1120	150	79	130
Density (kg/m^3)	2330	3440	2330	3100	2330
Π_1 (γ)	0.46958	0.40266	0.37156	0.34106	0.33505
Π_2 (γ)	0.31146	0.26661	0.24586	0.22554	0.22153
Π_5 (γ)	0.21798	0.18385	0.20752	0.16935	0.16619
Π_6 (γ)	1.37009	1.15544	1.30413	1.06410	1.04421
Π_7 (γ)	6.62385	7.16988	6.75023	7.50236	7.5872

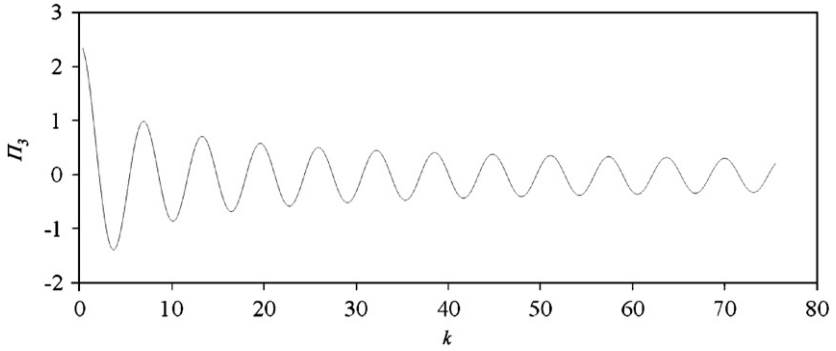

Fig. 9. The relation between the value of Π_3 and the wavenumber of the centers of the two clamped regions, corresponding to the case shown in Fig. 5(a).

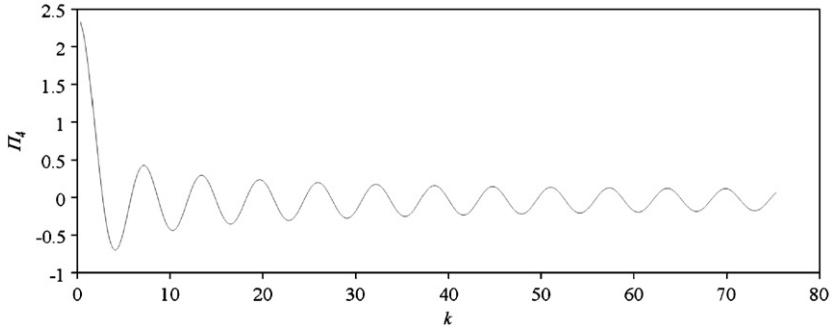

Fig. 10. The relation between the value of Π_4 and the wavenumber of the centers of the two clamped regions, corresponding to the case shown in Fig. 5(b).

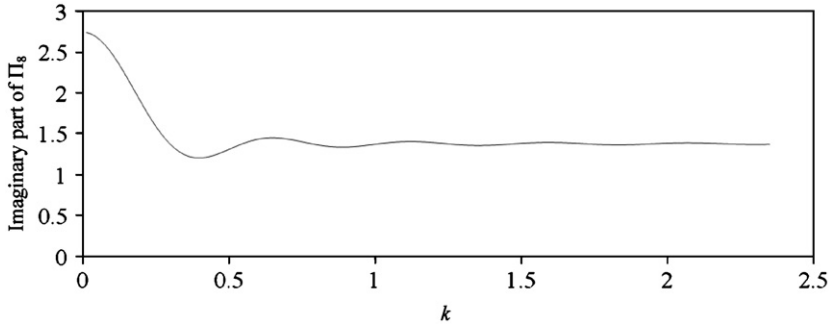

Fig. 11. The relation between the imaginary part of Π_8 and the wavenumber of the centers of the two clamped regions, corresponding to the case shown in Fig. 8(a).

6.3. Experimental verification

As expressed in Eq. (1), the measured quality factor of a micromechanical resonator vibrating in vacuum is the combination of the three loss mechanisms. Therefore, the quantitative experimental verification of the obtained expressions for the average vibration displacement on substrate is extremely difficult. Fortunately, as to the cases of the single shear stress and double stress sources shown in Figs. 4(a) and 5(a), respectively, the obtained expressions for their average vibration displacement on substrate have been quantitatively validated using systematical experimental data in Ref. [12], where TED and surface loss have also been simultaneously quantified. The accuracy of the derived expression for the case of a single circular normal stress source shown

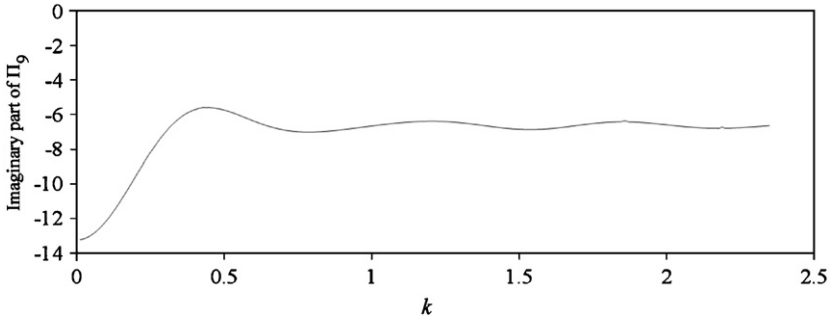

Fig. 12. The relation between the imaginary part of Π_9 and the wavenumber of the centers of the two clamped regions, corresponding to the case shown in Fig. 8(b).

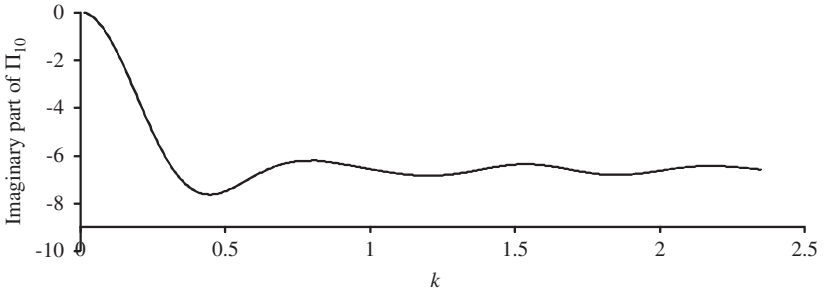

Fig. 13. The relation between the imaginary part of Π_{10} and the wavenumber of the centers of the two clamped regions, corresponding to the case shown in Fig. 8(c).

in Fig. 6 has been also quantitatively verified using experimental data of micromechanical disk resonators in Ref. [15], where TED and surface loss are not significant relative to support loss. The details about the experimental verification can be found in these two references. Since the same assumptions and methodology are employed to analyze the rest cases studied in this work, it is expected that the derived corresponding expressions for the average vibration displacement on substrate will also reflect reality. Certainly, the experimental study of the rest cases will help confirm their accuracy in the future.

7. Conclusion

This paper presents a comprehensive description of the vibration displacement on substrate under several typical time-harmonic stress sources in micromechanical resonators. Combined with the time-harmonic stress sources from a micromechanical resonator under study, the obtained mathematical expressions for the vibration displacement on substrate enable the quantitative evaluation of support loss in micromechanical resonators. Furthermore, the relation of support loss versus some key design parameters of a micromechanical resonator has been explored and offers the insights on design improvement for reducing support loss.

Acknowledgment

The authors would like to thank the reviewers for their valuable comments and suggestions that helped to improve the quality of this paper. This work is supported by National Science Foundation (NSF) under Grant No. 0826420.

References

[1] A.A. Seshia, M. Palaniapan, T.A. Roessig, R.T. Howe, R.W. Gooch, T.R. Schimert, S. Montague, A vacuum packaged surface micromachined resonant accelerometer, *Journal of Microelectromechanical Systems* 11 (2002) 784–793.

[2] M. Zaman, A. Sharma, Z. Hao, F. Ayazi, A mode-matched silicon-yaw tuning-fork gyroscope with subdegree-per-hour allan deviation bias instability, *Journal of Microelectromechanical Systems* 17 (2008) 1526–1536.

[3] N. Yazdi, F. Ayazi, K. Najafi, Micromachined inertial sensors, *Proceedings of the IEEE* (1998) 1640–1659.

[4] K. Wang, A.-C. Wong, C.T.-C. Nguyen, VHF free-free beam high-Q micromechanical resonators, *Journal of Microelectromechanical Systems* 9 (2000) 347–360.

[5] T. Mattila, O. Jaakkola, J. Kiihamaki, J. Karttunen, T. Lamminmaki, P. Rantakari, A. Oja, H. Seppa, H. Kattelus, I. Tittonen, 14 MHz micromechanical oscillator, *Sensors and Actuators A* 97–98 (2002) 497–502.

[6] L. Lin, R.T. Howe, A.P. Pisano, Microelectromechanical filters for signal processing, *Journal of Microelectromechanical Systems* 7 (1998) 286–294.

[7] C.T.-C. Nguyen, Frequency-selective MEMS for miniaturized communication devices, *Proceedings of IEEE Aerospace Conference* 1, Snowmass, Colorado, March 1998, pp. 445–460.

[8] T. Mattila, J. Kiihamaki, T. Lamminmaki, O. Jaakkola, P. Rantakari, A. Oja, H. Seppa, H. Kattelus, I. Tittonen, A 12 MHz micromechanical bulk acoustic mode oscillator, *Sensors and Actuators A* 101 (2002) 1–9.

[9] F.D. Bannon, J.R. Clark, C.T.-C. Nguyen, High-Q HF microelectromechanical filters, *IEEE Journal of Solid-State Circuits* 35 (2000) 512–526.

[10] C.T.-C. Nguyen, Micromechanical resonators for oscillators and filters, *IEEE Ultrasonics Symposium* 1 (1995) 489–499.

[11] K. Wang, C.T.-C. Nguyen, High-order medium frequency micromechanical electronic filters, *Journal of Microelectromechanical Systems* 8 (1999) 534–557.

[12] Z. Hao, A. Erbil, F. Ayazi, An analytical model for support loss in micromachined beam resonators with in-plane flexural vibrations, *Sensors and Actuators A* 109 (2003) 156–164.

[13] K.Y. Yasutnura, T.D. Stowe, E.M. Chow, T. Pfafman, T.W. Kenny, B.C. Stipe, D. Rugar, Quality factors in micron- and submicron-thick cantilevers, *Journal of Microelectromechanical Systems* 9 (2000) 117–125.

[14] J. Yang, T. Ono, M. Esashi, Energy dissipation in submicrometer thick single-crystal silicon cantilevers, *Journal of Microelectromechanical Systems* 11 (2002) 775–783.

[15] Z. Hao, F. Ayazi, Support loss in the radial bulk-mode vibrations of center-supported micromechanical disk resonators, *Sensors and Actuators A* 134 (2007) 582–593.

[16] H. Lamb, On the propagation of tremors over the surface of an elastic solid, *Philosophical Transactions of the Royal Society of London A* 203 (1904) 1–42.

[17] G.F. Miller, H. Pursey, The field and radiation impedance of mechanical radiators on the free surface of a semi-infinite isotropic solid, *Proceeding of the Royal Society of London* (1954) 521–541.

[18] K.F. Graff, *Wave Motion in Elastic Solids*, Ohio State University Press, Columbus, 1975.

[19] D.V. Jones, D. Le Houedec, M. Petyt, Ground vibrations due to rectangular harmonic loads, *Journal of Sound and Vibration* 212 (1998) 61–74.

[20] D.V. Jones, M. Petyt, Ground vibration in the vicinity of a rectangular load on a half-space, *Journal of Sound and Vibration* 166 (1993) 141–159.

[21] M.C. Cross, R. Lifshitz, Elastic wave transmission at an abrupt junction in a thin plate with application to heat transport and vibrations in mesoscopic systems, *Physical Review B* 64 (2001) 1–22.

[22] L.D. Landau, E.M. Lifshitz, *Theory of Elasticity*, Pergamon Press, London, 1959.

[23] D. Zwillinger, *Standard Mathematical Tables and Formulae*, Chapman & Hall/CRC Press LLC, Florida, 2003.

[24] J. Wang, J.E. Butler, T. Feygelson, C.T.-C. Nguyen, 1.51-GHz nanocrystalline diamond micromechanical disk resonator with material-mismatched isolating support, *Proceeding of the IEEE International Micro Electro Mechanical Systems Conference* (*MEMS'04*), Maastricht, The Netherlands, January 2004, pp. 641–644.

[25] Z. Hao, S. Pourkamali, F. Ayazi, VHF single crystal silicon elliptic bulk-mode capacitive disk resonators; Part I: design and modeling, *Journal of Microelectromechanical Systems* 13 (2004) 1043–1053.

[26] S. Pourkamali, Z. Hao, F. Ayazi, VHF single crystal silicon elliptic bulk-mode capacitive disk resonators; Part II: implementation and characterization, *Journal of Microelectromechanical Systems* 13 (2004) 1054–1062.